Local elastic response measured near the colloidal glass transition

D. Anderson, D. Schaar, H. G. E. Hentschel, J. Hay, Piotr Habdas et al.

Citation: J. Chem. Phys. **138**, 12A520 (2013); doi: 10.1063/1.4773220
View online: http://dx.doi.org/10.1063/1.4773220
View Table of Contents: http://jcp.aip.org/resource/1/JCPSA6/v138/i12
Published by the American Institute of Physics.

Local elastic response measured near the colloidal glass transition

D. Anderson,[1] D. Schaar,[1] H. G. E. Hentschel,[1] J. Hay,[1] Piotr Habdas,[2] and Eric R. Weeks[1]
[1]*Department of Physics, Emory University, Atlanta, Georgia 30322, USA*
[2]*Department of Physics, Saint Joseph's University, Philadelphia, Pennsylvania 19131, USA*

(Received 12 October 2012; accepted 10 December 2012; published online 7 January 2013)

We examine the response of a dense colloidal suspension to a local force applied by a small magnetic bead. For small forces, we find a linear relationship between the force and the displacement, suggesting the medium is elastic, even though our colloidal samples macroscopically behave as fluids. We interpret this as a measure of the strength of colloidal caging, reflecting the proximity of the samples' volume fractions to the colloidal glass transition. The strain field of the colloidal particles surrounding the magnetic probe appears similar to that of an isotropic homogeneous elastic medium. When the applied force is removed, the strain relaxes as a stretched exponential in time. We introduce a model that suggests this behavior is due to the diffusive relaxation of strain in the colloidal sample.
 [http://dx.doi.org/10.1063/1.4773220]

I. INTRODUCTION

Glass is an amorphous solid: despite the lack of long-range order, a glassy material is elastic rather than viscous. As a glass-forming material is cooled, its viscosity rises dramatically by many orders of magnitude; flow becomes difficult and slow. The elastic behavior of a glass, then, could be reframed as the material being probed on time scales too quickly for liquid-like flow to occur. The origins of this elasticity and the nature of the glass transition are active areas of research.[1–5] A related question is to what extent the macroscopic elastic behavior extends to the microscopic scale. For example, simulations have seen that the elastic moduli are spatially heterogeneous in some cases.[6,7] Certainly, the macroscopic elastic response treats the material as a continuum, whereas on a scale of the constituent molecules this could be a poor approximation.

Colloids are a simple model system which can be used to study the glass transition and the properties of glassy materials.[8–10] Colloidal suspensions are composed of solid particles in a liquid. The particles diffuse due to Brownian motion, but this diffusion is impeded at high particle concentration. In many experiments, colloidal particles only have short-range repulsive interactions, and the particles can be approximated as hard spheres.[11,12] In such samples the control parameter is the volume fraction ϕ and glasses are found for $\phi > \phi_g \approx 0.58$.[10,11] Near the glass transition, the viscosity rises quite dramatically, although some evidence suggests that perhaps it truly diverges at a point above ϕ_g.[13] In particular, an alternative divergence point is "random close packing" (rcp). This is the largest volume fraction possible for a sample that is still amorphously packed (rather than crystalline).[14] The volume fraction ϕ_{rcp} is known through simulations and taken to be $\approx$0.64, which agrees with early experiments done with ball bearings.[15]

Of course, the presence of the continuous liquid surrounding the colloidal particles is important for understanding the flow properties of colloids. Approaching the colloidal glass transition from $\phi < \phi_g$, samples are viscoelastic.[16] Their properties are described by both viscous and elastic moduli which are frequency-dependent. The viscosity mentioned above is understood to be the low-frequency limit. Indeed, if a glass is defined as an amorphous solid—a sample that does not flow—then it is important to recognize that whether or not its flow depends on the time scale of observation.[10]

While macroscopically one considers viscous and elastic behavior, microscopically one considers diffusion. A molecule or tracer particle in a fluid sample has a nonzero diffusion constant, which decreases to zero as the glass transition is approached. The decrease of the diffusion coefficient is attributed to caging. On short time scales, particles diffuse within a "cage" formed by their neighbors. On longer time scales, these cages rearrange and particles can move throughout the sample. As the glass transition is approached, the cage rearrangements occur less frequently, thus decreasing the diffusivity.[17–19] These cages provide a sort of elasticity for individual particles.[20–23] Particles which try to move away from the centers of their cages experience a restoring force.[18–20,23] If a constant external force is exerted on a particle, it will slowly move through the colloidal suspension as cages rearrange, although the force needs to be kept small when ϕ is close to ϕ_g to avoid nonlinear behavior.[24–28] If a sufficiently high external force is applied to a particle, it can break the cages and move through the sample more freely (typically with a nonlinear relationship between the force and resulting velocity),[26,27,29–33] disturbing and rearranging particles as it moves.[29,34]

In this paper we probe the elastic response of a dense colloidal suspension by locally exerting a small force on a magnetic bead. Our studies are conducted on a time scale faster than the sample can relax due to diffusion. We find that the sample responds elastically, with a Young's modulus E that rises as the glass transition is approached, and a Poisson ratio σ equal to 1/2. We also study the relaxation of the magnetic bead after it has been displaced and the force removed.

This relaxation is faster for higher volume fraction samples. We present a model that captures the stretched exponential character of the relaxation, by assuming that in our colloidal sample stress diffuses away to infinity at long times.

II. EXPERIMENTAL METHODS

The colloidal suspensions are made of poly-(methylmethacrylate) particles, sterically stabilized by a thin layer of poly-12-hydroxystearic acid.[35] The particles have a radius $a = 1.55$ μm, a polydispersity of ~5%, and are dyed with Rhodamine.[36] The uncertainty of the mean particle radius is ± 0.01 μm. The particles are slightly charged, but their glass transition is still at $\phi_g = 0.58 \pm 0.01$, signaled by the diffusion of particles going to zero on experimental time scales (several hours). The colloidal particles are suspended in a mixture of cyclohexylbromide/*cis*- and *trans*-decalin, which nearly matches both the density and the index of refraction of the colloidal particles.[36] The density of this solvent is 1.232 g/cm^3, the index of refraction is 1.495, and the viscosity is $\eta = 2.18$ mPa s. The particles are fluorescently labeled for visualization.[36] Before beginning experiments, we stir the sample with an air bubble to break up any pre-existing crystalline regions, then wait 20 minutes before taking data.

A small quantity of superparamagnetic beads (Dynal M450, coated with glycidyl ether reactive groups) with a radius of 2.25 μm is added to the colloidal suspension. We do not observe attraction or repulsion between the colloidal particles and the magnetic beads, in either dilute or concentrated samples. The beads are not completely monodisperse in their magnetic properties, and our calibration finds the variability in the effective magnetic force applied to different beads to be less than 10%. Also, the magnetic beads are not density matched, and their effective weight is 0.1 pN. This is a factor of ten smaller than the smallest horizontally applied magnetic forces in our experiments. We study isolated magnetic beads at least 35 μm from the sample chamber boundary and from other magnetic beads.

For some of the data (Fig. 1, in particular), we use a conventional Leica DMIRB inverted microscope with a CCD camera. A magnetic bead appears as a large dark circle in our images and its position as a function of time is found using standard particle tracking techniques.[37] For these experiments, the typical image size is 15×40 μm^2, with images taken at a rate of 30 frames per second. The magnetic bead position is resolved to within 0.04 μm.

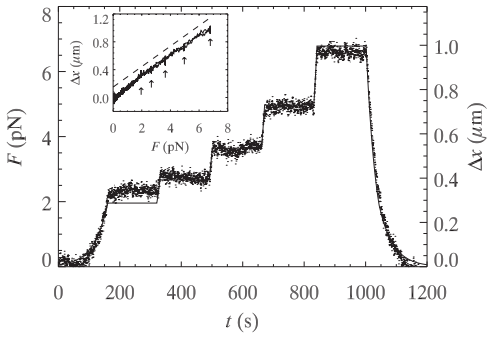

FIG. 1. The solid line indicates the applied force as a function of time. The points show the measured displacement Δx of the magnetic bead. (Inset) Same data plotted as Δx against F. The dashed line is a fit to the data, with the slope leading to an effective spring constant $k = 6.8 \pm 0.1$ pN/μm, offset vertically for clarity. The arrows indicate locations where the force was held constant. The volume fraction is $\phi = 0.55$.

For other data, we use a ThermoNoran Oz confocal microscope. With this microscope, we acquire images of area 80 μm $\times$ 75 μm at a rate of 30 frames per second (256 $\times$ 240 pixels^2). The magnetic beads are not fluorescent and thus appear black on the background of dyed colloidal particles (see Fig. 3). Our particle tracking resolution is 0.05 μm for the magnetic beads. With either the confocal microscope or the video microscope, we only track the motion of particles in 2D: for the experiments in this paper, the magnetic particle position always remains with the imaging plane of the microscope.

We additionally use the confocal microscope to take three-dimensional images of these samples to determine the volume fraction.[36] We count the particles within the imaged volume, and convert from the measured number density n to volume fraction ϕ using $\phi = (4\pi/3)na^3$. Due to our uncertainty of the mean value of the particle radius a, we have a systematic uncertainty of 2% of our ϕ values.[38] That is, our ϕ values are fairly accurate when compared with each other, but a reported value of $\phi = 0.50$ is uncertain by ± 0.01.

We use a strong neodymium permanent magnet mounted on a micrometer positioner to control the force applied to the magnetic beads. The micrometer accurately reproduces the magnet position and thus our uncertainty in the force between different experiments is limited by the magnetic bead variability, rather than the magnet positioning. For many experiments, a computer-controlled stepper motor attached to the micrometer allows us to slowly and controllably vary the applied force over two orders of magnitude.

For other experiments, we want to apply a short-duration magnetic force. We mount the magnet on a linear actuator (Ultra Motion D-A.25-HT17). The magnet is then brought close to the magnetic bead resulting in a high force acting on the magnetic bead for a short time; the details are discussed below.

Our experiments are controlled-force experiments, in contrast to controlled displacement.[39,40] For example, this means that particles do not necessarily need to move in the direction of the applied force, although we discuss below that they appear to always do so. Prior work by other groups used laser tweezers to move probe particles through colloidal suspensions at a controllable velocity,[41–44] finding many interesting results such as anisotropy of the disturbed region around the moving particle[41] and a decoupling of structural and hydrodynamic influences on the particle motion.[44] These prior experiments studied probe particles as they moved over long distances, in contrast to our experiments described below where the magnetic bead always remains close to its equilibrium position.

III. LINEAR ELASTIC RESPONSE

In our earlier work, we applied a constant force and observed the steady-state motion of the magnetic bead.[30] For

large forces, the velocity of the magnetic bead grew nonlinearly with increasing force, consistent with shear-thinning. We also observed that the velocity was essentially zero below a threshold force. The threshold force grew dramatically as the glass transition was approached.[30]

To test the behavior of the sample below the threshold force for motion, we vary the magnetic force within a range of forces that are below the threshold force for motion. To ensure that the forces used are below the threshold force for motion, each increase in the force was followed by a waiting period of 160 s to observe the subsequent motion of the magnetic bead. The applied force as a function of time is shown in Fig. 1 by the solid line. In this situation, the magnetic bead has a finite displacement, rather than a finite velocity; the displacement is shown by the dots in Fig. 1. As the figure shows, by appropriately rescaling the units, the displacement of the magnetic bead from its original position is linearly proportional to the applied force. Additionally, during each of the pauses at constant force, the magnetic bead exhibits slight fluctuations around its equilibrium position. Some of this is due to Brownian motion, and some of this is due to the uncertainty in identifying the position of the magnetic bead ($\sim$0.04 μm).

Further evidence for the linearity is seen in the inset of Fig. 1, showing the displacement data plotted as a function of the applied force. The data are linearly related, and a fit to the data leads to an effective spring constant $k = 6.8$ pN/μm. The arrows shown in the figure indicate locations where the magnetic force was constant. This spring constant is quite large: a reasonable comparison can be made with the thermal energy k_BT and the radius of the colloidal particles a, and working through the change of units 6.8 pN/μm $= 4000k_BT/a^2$.

IV. PARTICLE DISPLACEMENT FIELDS

Unfortunately, the results of Fig. 1 are atypical in one important respect: for many experiments lasting longer than O(100 s), the magnetic bead experiences a cage rearrangement and does not return to its original position. The spring constant before and after any such displacement is always the same, to within our uncertainty. Accordingly, to complement the slow experiments of Fig. 1, we conduct experiments with intermittent and short pulses of force to see the instantaneous response of the sample on a time scale quicker than cage rearrangements. A nondimensional way to consider this is the modified Peclet number.[30] Pe^* is the ratio of the time it would take for a colloidal particle to diffuse its own size to the time scale for the perturbation. The diffusive time scale is $\sim$400–5000 s for the samples we study ($\phi > 0.4$), and the perturbation time scale is 0.25 s. Thus, $Pe^* \approx$ 2000–20 000, signifying that Brownian motion is unimportant on the time scales we study: particles do not substantially rearrange their positions during our experiment. The recovery to the perturbation (discussed in Sec. V) takes O(10 s), which is still in the high Pe limit.

To discover the origin of the linear restoring force, we examine the response of the colloidal particles surrounding the magnetic bead. To produce reproducible initial strains, we attach the external permanent magnet to a linear actuator as described in Sec. II, and move the magnet toward the sample and then away at maximum speed. The force applied is ramped up to a maximum value and then just as rapidly reduced. To calibrate the force as a function of time, $F(t)$, we use this procedure to exert a force on magnetic beads suspended in glycerol. Such beads move with velocity $v(t)$, from which we deduce the force $F(t)$ using Stokes' Law, $F = 6\pi\eta a_{\mathrm{MB}} v$, with the viscosity of glycerol $\eta = 0.934$ Pa s. The resulting $F(t)$ data are plotted in Fig. 2 for the three largest $F_{\max}$. These correspond to the cases where the external magnet is moved the closest to the sample. For example, the top curve in Fig. 2 takes longer to reach its peak and longer to return to $F = 0$, as the magnet has farther to move.

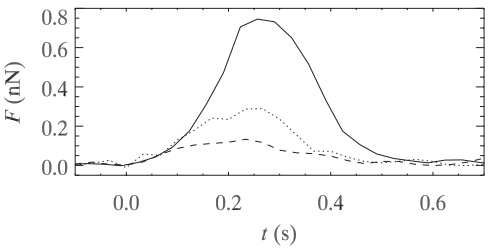

FIG. 2. Applied force as a function of time, for the three largest maximum forces (see Table I). For all curves, $F(t) = 0$ for $t < 0$ s.

The peaks of the curves, $F_{\max}$, are confirmed by measuring the velocity of magnetic beads in glycerol while the external magnet is fixed in its closest distance to the sample for a given forcing protocol. Those results agree quite well with the values measured from the $F(t)$ data. In the results that follow, we refer to the different $F(t)$ by their maximum values $F_{\max}$ which are listed in Table I. An additional way to quantify the $F(t)$ is by their time integral, $I = \int F(t)dt$, yielding an impulse which is applied to the magnetic bead. These values are also listed in Table I. In each case, the ratio $I/F_{\max} = 0.25 \pm 0.03$ s, suggesting that our choice of using $F_{\max}$ is correctly representing I as well, and that the effective pulse duration is a quarter of a second. This time scale is short compared to the Brownian time scale $a_{\mathrm{MB}}^2/D_{\mathrm{MB}} = 110$ s. (To compute this time scale, we use $D_{\mathrm{MB}} = k_BT/6\pi\eta a_{\mathrm{MB}}$ with η being that of the solvent, that is, we are using the $\phi \to 0$ value for the diffusion constant.)

The response of the sample to a pulse is shown in Fig. 3(b). This is a difference image formed by subtracting the raw image before the pulse (such as Fig. 3(a)) from the raw image after the pulse. In this case, the magnetic particle has

TABLE I. The five different maximum forces applied, and the integrated impulse $I = \int F(t)dt$. The calibration procedure (described in the text) has an intrinsic $F_{\max}$ uncertainty of $\pm$0.05 nN and an I uncertainty of $\pm$0.005 nN s. Due to variability between different magnetic beads, for a given magnetic bead there is also an overall systematic uncertainty of $\pm$10%. Graphs of $F(t)$ for the three largest values of $F_{\max}$ are shown in Fig. 2.

$F_{\max}$ (nN)	I (nN s)
0.042	0.011
0.077	0.020
0.13	0.036
0.29	0.068
0.75	0.17

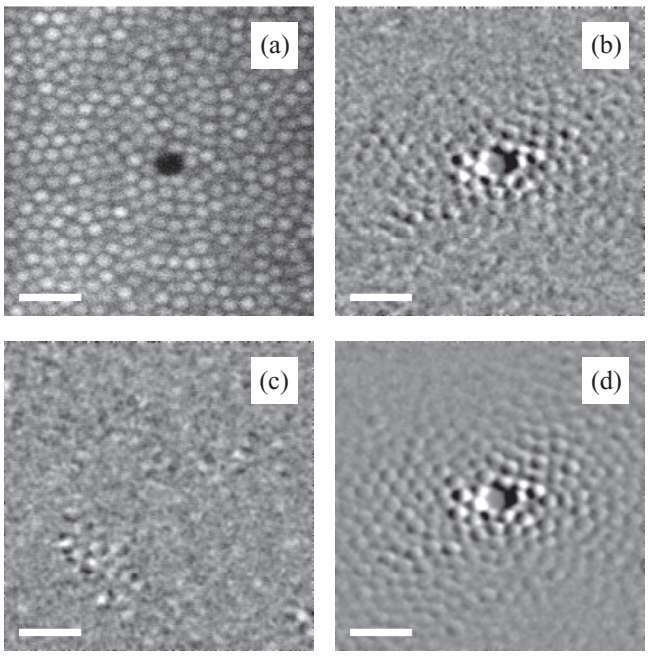

FIG. 3. (a) Raw image of particles, before the force is applied. (b) Difference between "before" and "after" a single force pulse is applied. (c) Difference between two "after" images for two subsequent pulses. (d) As the images are reproducible, a sequence of eight "before" pictures is averaged together, and likewise eight "after" pictures. This picture is the difference between these average images. For all pictures, the scale bar is 10 microns long, the volume fraction is $\phi = 0.49$, and the applied force is $F_{\max} = 0.29$ nN.

moved to the left, as indicated by the white crescent on its left side. Because the magnetic bead is black and the colloids are white, the colloidal motion is indicated by the direction of the black crescents, and is also clearly leftward. Furthermore, the overall disturbed region of colloids is a fairly smooth function of space. Adjacent colloids move similar distances in Fig. 3(b).

This displacement field is highly reproducible, as is shown by creating a difference image in Fig. 3(c) between two images both taken when the colloids are maximally displaced from their equilibrium positions. The difference image is nearly completely gray showing that the displacements are virtually the same. Slight local variations are due to Brownian motion of particles within their cages, but no rearrangements occur over the duration of the experiment. Due to the reproducibility of the experiment, it is reasonable to average the images "before" and the images "after" to reduce the variability caused by Brownian motion. The resulting difference image is shown in Fig. 3(d) and emphasizes the smoothly spatially varying displacements of the colloids. It can be seen that the applied force is not exactly on the x-axis of the image; this is dealt with in the analysis below.

To quantify the images shown in Fig. 3, we perform particle image velocimetry (PIV) on the pairs of "before" and "after" images. This method is frequently used in experimental fluid mechanics, and does not depend on identifying or tracking individual particles.[45] A small window in the first image is taken, and cross-correlated with the same size window in the second image. By moving the second window around in the second image, we find which piece of the second image is best correlated with the piece from the first image. The shift required for this maximum correlation is a displacement vector reflecting how the particles have moved between the two images, and, in particular, represents the displacement vector for the center of the window. We use a window size that roughly encompasses two particles, although our results are not sensitive to this choice. The technique is merely correlating the images and the particles provide contrast to help this work. A typical displacement field is shown in Fig. 4(a), corresponding to the images shown in Figs. 3(a) and 3(b). For the PIV analysis, we use the individual raw images such as Fig. 3(a) which leads to Fig. 3(b), rather than the averaged images which lead to Fig. 3(d). After computing the PIV analysis for each individual pulse, we average the PIV fields over the pulse sequence for a given $F_{\max}$ and ϕ to do the subsequent analysis.

The smoothly varying appearance of the displacement field seen in Fig. 4(a) suggests trying to fit the strain field to a simple functional form. As noted previously, the response of the magnetic bead to a constant force is a simple linear function, and so a natural choice is to treat the colloidal suspension as a homogeneous elastic medium. In such a medium, the strain field $\vec{u}$ around a point force $\vec{F}$ applied at the origin is given by[46]

$$\vec{u} = \frac{1}{8\pi Er}\frac{1+\sigma}{1-\sigma}[(3-4\sigma)\vec{F} + \hat{n}(\hat{n}\cdot\vec{F})], \qquad (1)$$

where E is the Young's modulus, σ is the Poisson ratio, and $\hat{n}$ is a unit vector pointing away from the origin. Using $\hat{n} = \hat{x}\cos\theta + \hat{y}\sin\theta$ and $\vec{F} = F\hat{x}$, the equation can be rewritten as

$$\vec{u} = \frac{1}{16\pi r}\left(\frac{F}{E}\right)\left(\frac{1+\sigma}{1-\sigma}\right)[(7-8\sigma+\cos 2\theta)\hat{x} + (\sin 2\theta)\hat{y}], \qquad (2)$$

which highlights the key spatial dependence of the strain field: it decays as $1/r$, and has a periodic dependence on 2θ, due to the symmetry of the problem about the x-axis. $\theta = 0$ corresponds to the direction of the force.

To test this, we rescale the displacements u_x and u_y (measured from PIV) by r. This collapses the data reasonably well, as shown in Fig. 5. Here the data are plotted as a function of θ, showing the characteristic modulation in Eq. (2). The solid line in Fig. 5 is a fit to the equation. The amplitude of both fit curves is constrained by the model to be the same, which is in slight disagreement with the raw data, where $u_x r$ is somewhat larger in amplitude than $u_y r$. This is seen in most of our data sets. The curve for $u_x r$ is vertically offset from zero, and it can be seen from Eq. (2) that the magnitude of the offset is related to the Poisson ratio σ.

The fit has several parameters. First, the direction for $\theta = 0$ is chosen to be the average direction of all of the displacement vectors to correct for the imperfect magnet alignment. Second, the two physical parameters to the fit are σ and E. A difficulty in determining E is that the true value of F is unknown: the model assumes a steady F, whereas we apply a pulse. If the force was held at $F_{\max}$, the magnetic bead would move with a velocity and would not return to its original position, given the large values of $F_{\max}$ we use.[30] Fortunately, $\vec{u}$ scales reasonably well with $F_{\max}$ and thus leads to a consistent value for the Young's modulus E, even if its true

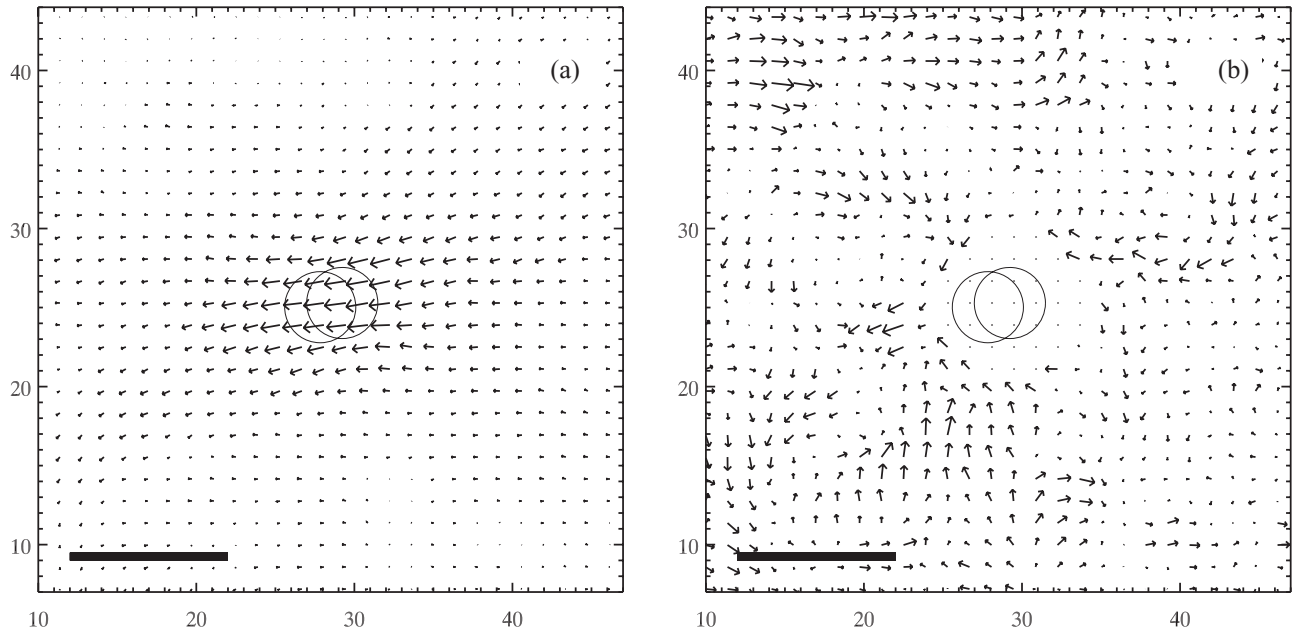

FIG. 4. (a) Displacement field based on data shown in Fig. 3(b). The arrows indicate displacements of the colloidal particles. (b) Residual displacement field after subtracting off the fit to Eq. (2). The arrows are magnified by a factor of 5; in reality, the longest displacement vectors in panel (b) are 0.3 μm. The central region near the magnetic bead is removed for clarity. For both panels, the circles indicate the initial and final positions of the magnetic bead, which moved from right to left, and are drawn to scale. The scale bar is 10 microns long. The data correspond to Figs. 4 and 5: $\phi = 0.49$ and $F_{\max} = 0.29$ nN. Note that a displacement vector is calculated for every pixel in the raw images; here, only every 6th vector is drawn.

magnitude cannot be deduced from our fits. Third, we allow for the location of the origin ($x = 0$, $y = 0$) to vary. It is not obvious if the origin should be at the starting position of the magnetic bead, the ending position, or elsewhere, especially given that the magnetic bead is a finite-sized disturbance and the model assumes a point-sized disturbance. We adjust the origin so that the model has the best fit to the data; this typically puts the origin within 0.3 μm of the starting position of the magnetic bead. A final parameter to our fitting algorithm is above what radius r_0 from the magnetic bead the fitting is conducted. Sufficiently close to the magnetic bead, its finite size begins to distort the strain field from the model. We fix $r_0 = a_{\mathrm{MB}}$, and in practice our results are not sensitive to our choice.

Despite the slight disagreements between the raw data and the model shown in Fig. 5, overall the model is remarkably successful. For a few samples, we find that the Young's modulus E increases slightly with increasing $F_{\max}$, but more often we find E is independent of $F_{\max}$ and accordingly for each sample we average E over the different trials with different $F_{\max}$. The resulting data are plotted in Fig. 6, and E increases by a factor of ~8 as the glass transition is approached. Simulations and theory show that elastic moduli diverge near the jamming transition as $B \sim (\phi_c - \phi)^{-\beta}$ with $\phi_c \approx 0.64$, the volume fraction of random close packing.[47–50] The exponent β depends on the details of the interparticle interaction and on which modulus is considered. The inset of Fig. 6 shows E plotted as a function of $(\phi_c - \phi)$ with behavior consistent with a power-law, although our data extend over only half a decade of $(\phi_c - \phi)$. Our exponent is $\beta = 1.84 \pm 0.40$, similar to results for the bulk modulus of hard spheres ($\beta = 2$) and shear modulus of hard spheres ($\beta = 3/2$).[50]

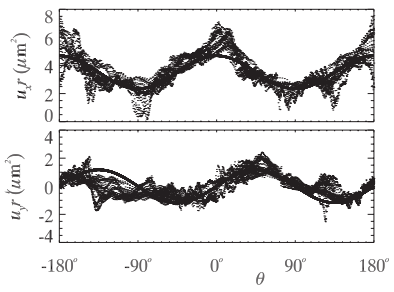

FIG. 5. Rescaled displacement vectors as a function of θ; compare with Eq. (2). The points are the data and the solid line is the fit to the equation. The data correspond to Figs. 3(b) and 4(a), using only data with $r > r_0 = a_{\mathrm{MB}}$. For this fit, σ was constrained to be 1/2.

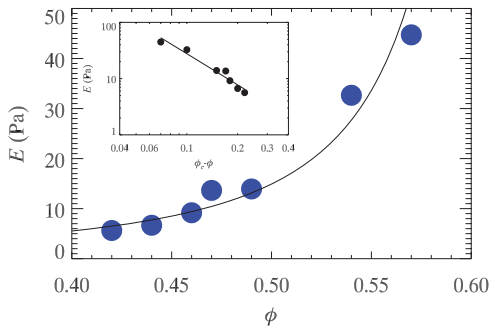

FIG. 6. Young's modulus E as a function of volume fraction ϕ. Due to an inadequately defined applied force, E is overestimated although this affects all points equally (by a multiplicative factor) and does not change the shape of the curve; see the text for a discussion. The inset shows the same data plotted as a function of $\phi_c - \phi$ with $\phi_c = 0.64$. The lines in the main plot and the inset are the fit to the data using $E = E_0(\phi_c - \phi)^{-\beta}$ with $E_0 = 0.4$ Pa and $\beta = 1.84 \pm 0.40$. The symbol size indicates the uncertainty.

Our values of E are quite similar to those found in a classic study of viscoelastic shear moduli of colloidal supercooled liquids,[16] although that is a coincidence. On the one hand, Eq. (2) assumes the sample is in equilibrium for the applied force, which is certainly not the case. Using $F_{\max}$ overestimates E. On the other hand, our particles are 7.4 times larger than those of Ref. 16, so our moduli should be smaller by a factor of $7.4^3 = 400$. We can estimate the correct order of magnitude for our data from Fig. 1, using Eq. (2) with our effective spring constant $k = 6.8$ pN/μm (setting this equal to u/F) and $r = a_{\mathrm{MB}} = 2.25$ μm. This gives us $E = 0.72$ Pa for $\phi = 0.55$, suggesting that our data in Fig. 6 are overestimated by a factor of $O(100)$. Thus, we are in plausible agreement with the data of Ref. 16 in the high-frequency limit, in particular, which is most relevant for our quickly perturbed samples.

An alternative comparison for E can be made with the theory of Schweizer and Saltzman, who developed an effective "free energy" for a hard sphere trapped in a cage.[20] They construct the free energy $F(r)$ as a function of the distance r from the cage center. For particle motion within the cage, they find an effective spring constant depending on ϕ as $k \sim k_0 \exp(25.3\phi)$ with $k_0 = 2.5 \times 10^{-4} k_B T/a^2$ (where k_B is Boltzmann's constant, T is the absolute temperature, and a is the colloidal particle radius). In our experiment, the magnetic bead is larger than the surrounding particles by a factor of 1.45, so the effective spring constant experienced by our bead will be larger by $1.45^2 = 2.1$. Using $\phi = 0.55$ and correcting for the bead size, their theory predicts $k \approx 580 kT/a^2$, as compared to our result of $k = 6.8$ pN/μm $= 4000 k_B T/a^2$. Our result is a factor of 7 larger. Overall, given the approximations made by the theory and the uncertainties of the experiment, agreement within a factor of 7 is suggestive that the origin of the elasticity we observe is indeed the caging of the particles. Recent work by Harrer *et al.*[23] combined mode coupling theory and simulations, and also found somewhat smaller spring constants than we do, $\approx 150 k_B T/a^2$ for $\phi = 0.55$, or $320 k_B T/a^2$ after adjusting for the magnetic bead size. Interestingly, Harrer *et al.*[23] also found a "strain softening" effect (decreasing spring constant) at large applied forces $F \gtrsim 5 k_B T/a$.[23] Figure 1 shows forces up to 7 pN $= 2600 k_B T/a$ without any strain softening; however, as noted above, Fig. 1 is an atypical result and most magnetic beads under these forces move out of their cages, in agreement with the predictions of Ref. 23.

The other key fit parameter in Eq. (2) is the Poisson ratio σ. For all $F_{\max}$ and ϕ, we find $\sigma = 0.50 \pm 0.08$. Values of σ larger than 1/2 are unphysical, so we conclude that our data show $\sigma = 1/2$. Accordingly, we fix this value and redo the fits to Eq. (2), and the values of E that result are the ones shown in Fig. 6 and correspond to the fit curves shown in Fig. 5. The physical meaning of $\sigma = 1/2$ is that volume is conserved during deformation: if this sample is strained in one direction, the sides contract sufficient to conserve volume. This is plausible, as the sample itself is an incompressible fluid with solid particles, and additionally one assumes the volume fraction stays homogeneous during simple deformations.

As noted above, we allow the direction of the force to be a free parameter when performing the fit. This angle is fairly constant, with a standard deviation of only 4° between the different experiments. This variability likely reflects measurement error.

The fit shown in Fig. 5 is not perfect, and some systematic deviations from the fit can be seen. The difference between the fit and the measurements is shown in Fig. 4(b). The displacement vectors are stretched by a factor of 5, and thus greatly exaggerate the difference. Nonetheless, this picture looks similar to the locally nonaffine elastic behaviors seen in some simulations[6,51–53] and also images of "floppy-modes," localized normal modes, and "soft spots" known to be present near jamming.[54–58] We stress that the majority of the total displacement field shown in Fig. 4(a) is well-fit by Eq. (2).

V. DECAY OF STRAIN

A. Experimental observations

After the force is removed, the magnetic bead moves back to its equilibrium position. Typical data of the magnetic bead displacement as a function of time are shown in Fig. 7(a). Within our resolution, the magnetic bead is always in the initial position less than 10 s after it starts the return motion.

Figure 7(b) shows the data on a semilog plot, where straight lines would indicate exponential decay. While the initial portion of the data can be fit to straight lines, clear deviations are seen at longer times. The decay times found are 0.3–0.5 s but do not depend systematically on the initial displacement. Furthermore, some evidence of memory is seen. For example, the $F_{\max} = 0.29$ nN data (green triangles) go from $x = 2.0$–0.4 μm during the time interval $t = 0.0$–0.7 s. In contrast, the $F_{\max} = 0.75$ nN data (red squares) go from

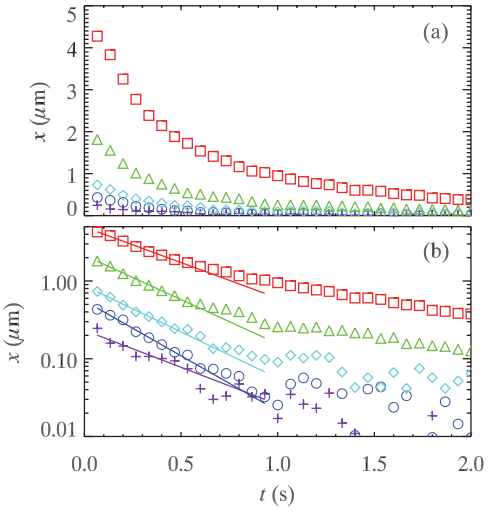

FIG. 7. Plots of the displacement of the magnetic bead as a function of time, after the force is removed, for $\phi = 0.49$. Panel (a) shows a linear-linear plot and panel (b) shows a log-linear plot. The values of $F_{\max}$ are given in Table I, with the largest initial displacement (red squares) corresponding to the largest force and the smallest initial displacement (purple pluses) corresponding to the smallest force. In (b), lines are fit to the initial data ($t < 0.5$ s) indicating decay time constants of 0.47 s, 0.38 s, 0.37 s, 0.31 s, and 0.46 s (from largest $F_{\max}$ to smallest).

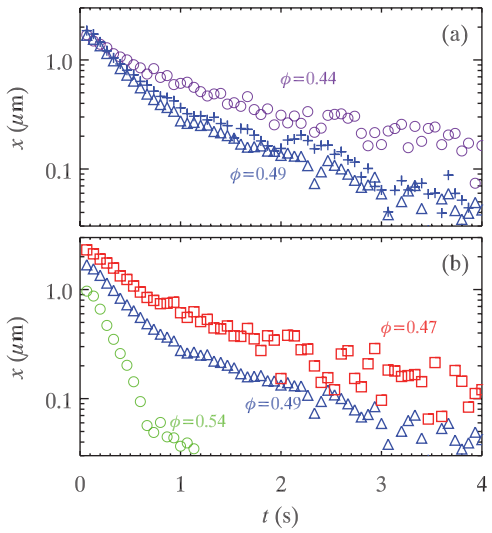

FIG. 8. Relaxation curves for several experiments demonstrating that the decay is faster for samples with higher ϕ. (a) Comparison of two samples with ϕ as indicated that have nearly the same initial displacement. For the $\phi = 0.44$ data, the force is $F_{max} = 0.13$ nN, and for the $\phi = 0.49$ data, the force is $F_{max} = 0.29$ nN. Two different instances are shown for the $\phi = 0.49$ data (triangles and pluses). (b) Comparison of three samples with the same force ($F_{max} = 0.29$ nN) but different ϕ as indicated.

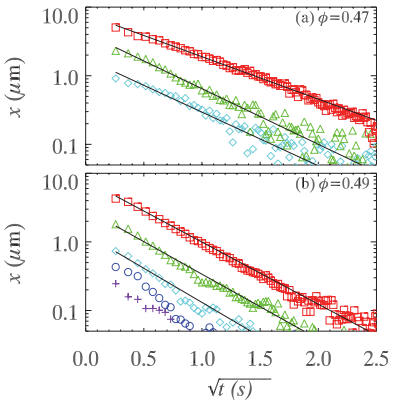

FIG. 9. Displacement plotted as a function of $\sqrt{t}$ for (a) $\phi = 0.47$ and (b) $\phi = 0.49$. The different symbols indicate different values of F_{max}. The values of F_{max} are given in Table I, with the largest initial displacement (red squares) corresponding to the largest force and the smallest initial displacement (purple pluses) corresponding to the smallest force. The straight lines indicate fits to $\sim\exp(-\sqrt{t/t_0})$. For (a), the values of t_0 are 0.50, 0.29, and 0.31 s (top to bottom). For (b), the values of t_0 are 0.23, 0.21, and 0.19 s (top to middle).

$x = 2.0$ to 0.4 μm during the time interval $t = 0.4$–1.9 s, taking nearly twice as long to cover the same displacement. The noisy data seen in Fig. 7(b) at small values of x are partly due to the uncertainty in determining x (± 0.04 μm). The $x = 0$ position is defined by an average at long times and so is more accurately defined. Within our resolution the positions shown in Fig. 7(b) have not quite decayed to $x = 0$ over the time period shown.

One trend is that samples with larger ϕ (closer to the glass transition) decay faster, as is shown in Fig. 8. Given the nontrivial memory effects, it is not obvious whether to compare data at constant initial displacement or at constant F_{max}. This distinction turns out to be unimportant. Figure 8(a) compares two different volume fractions with the same initial displacement, and the data at larger ϕ decay faster. Figure 8(b) shows three different volume fractions with the same F_{max}, with the same trend, data for larger ϕ decay faster. This makes intuitive sense, as the elastic modulus is larger for larger ϕ (Fig. 6). While viscous dissipation rises as the glass transition is approached,[16] apparently the elastic contribution to the magnetic bead relaxation rises faster, resulting in a faster relaxation.

While the position as a function of time does not appear to decay exponentially (Fig. 7), plotting the data in Fig. 9 as a function of $\sqrt{t}$ suggests $x \sim \exp(-\sqrt{t/t_0})$. The value of t_0 is slightly larger for larger initial displacements, although the data in Fig. 7 are fairly parallel within each panel, showing that t_0 is not changing that dramatically. t_0 is clearly larger for lower volume fractions ϕ.

B. Model of relaxing bead

To explain the stretched exponential decay process, we develop a model that treats the relaxation of stresses in the viscoelastic colloidal sample. Consider the relaxation dynamics of a magnetic bead of radius a_{MB} initially at $x = 0$ in a viscoelastic medium that is suddenly displaced at time $t = 0$ by an amount x_0 due to an imposed force F. The bead was originally (at $t < 0$) in equilibrium and the displacement will result both in a force exerted on the external medium by the bead creating a stress field in the colloidal medium and a reaction force by this medium on the bead. The experiments show clearly the presence of both memory and a stretched exponential behavior for the bead relaxation. We show here that if the induced stress field relaxes in a diffusive manner then such behavior arises. The reaction force will thus in general be a function of both the applied force F that creates the inhomogeneous stress field around the bead, as well as time t due to diffusive relaxation of the stress field. This reaction force will tend to bring the bead back to its original equilibrium position due to the elastic forces exerted on the bead together with a viscoelastic drag force that will dissipate energy. Thus, we can write the equation of motion,

$$m\ddot{x} = -m\int_0^t \zeta(t-s)\dot{x}(s)ds - k(F,t)x, \qquad (3)$$

where the first term on the RHS is the viscoelastic drag on the bead and the second term represents the elastic force on the bead in the presence of a relaxing force constant $k(F, t)$. Because the motion is slow, we can replace the viscoelastic drag by its viscous zero frequency limit. Namely, defining $\gamma = \int_0^\infty \zeta(t)dt$, we can rewrite Eq. (3) as

$$\ddot{x} = -\gamma\dot{x} - \omega(F,t)^2 x. \qquad (4)$$

We estimate $\gamma = 6\pi a_{MB}\eta/m$ using Stokes' law with η being the effective viscosity of the colloidal medium, and we define $\omega(F, t)^2 = k(F, t)/m$.

Our first challenge is to estimate $k(F, t)$. We can see from the strain field $u(\mathbf{r})$ induced in the colloidal medium due to the applied force F (see Eq. (1)) that there exists a length scale ξ_0 over which the colloidal displacements will be greater than the typical colloidal particle radius a. This scale can be

estimated as

$$\xi_0(F) \approx CF/(Ea), \tag{5}$$

where E is the Young's modulus of the sample and the constant $C \approx (1/16\pi)(1+\sigma)(7-8\sigma)/(1-\sigma) \approx 0.2$. Using our largest $F_{\max} = 0.75$ nN and $E \approx 15$ Pa, $\xi_0 \approx 4a$. Given that the medium is not perfectly elastic but rather viscoelastic, we argue that this region grows diffusively as the strain is dissipated in the surrounding medium, leading to a growing length scale $\xi(F, t)$, where

$$\xi(F,t)^2 = \xi_0(F)^2 + 6Dt. \tag{6}$$

In Eq. (6), D is the diffusion constant characterizing motion that can relax the strain, which does not require cage rearrangements. We discuss D in more detail below. Using $\xi(F, t)$ we can estimate the typical strains in the colloidal medium induced by the bead. These strains, $\epsilon \approx x/\xi(F, t)$, reduce with time both due to the diffusive relaxation of the initial strain and the reduced imposed forces, as the bead returns to its original equilibrium position. The associated elastic stresses in the colloid are then $\approx Ex/\xi(F, t)$. Thus, we are now in a position to estimate the restoring force on the bead as $k(F, t)x \approx 4\pi R^2 Ex/\xi(F, t)$ or

$$\omega(F,t)^2 \approx 4\pi R^2 E/(m\xi(F,t)) = \omega_0^2/\sqrt{(1+t/\tau)}, \tag{7}$$

where $\omega_0^2 = 4\pi R^2 E/(m\xi_0(F))$ and $\tau = \xi_0(F)^2/6D$. Substituting Eq. (7) into Eq. (4) then yields

$$\ddot{x} = -\gamma\dot{x} - \omega_0^2 x/\sqrt{(1+t/\tau)}. \tag{8}$$

The relaxational behavior of the bead can now be found by solving Eq. (8) subject to the initial conditions $x(t=0) = x_0$ and $\dot{x}(t=0) = 0$. Though Eq. (8) cannot be solved exactly, it has two limiting forms. For $t \ll \tau$, Eq. (8) reduces to $\ddot{x} = -\gamma\dot{x} - \omega_0^2 x$. This is the equation of motion for a linear oscillator with two overdamped modes,

$$x(t) = (x_0/2)\{\alpha_+ \exp[-\gamma\alpha_- t/2] + \alpha_- \exp[-\gamma\alpha_+ t/2]\}, \tag{9}$$

using $\alpha_\pm = 1 \pm \sqrt{1-4\omega_0^2/\gamma^2}$. In the limit $t \gg \tau$, Eq. (8) reduces to $\ddot{x} = -\gamma\dot{x} - \omega_0^2\sqrt{\tau/t}x$. In this limit, we have a stretched exponential solution,

$$x(t) \approx (x_0/2)\alpha_+ \exp(-\sqrt{t/t_0}), \tag{10}$$

where $t_0 = \gamma^2/(\omega_0^4\tau) = (27/2)\eta^2 D/(a_{\mathrm{MB}}^2 E^2)$. Significantly, t_0 does not depend on the initial displacement x or on the initial applied force F.

We can compare these predictions to the experiment. As mentioned above, using $F_{\max} = 0.75$ nN and $E \approx 15$ Pa, $\xi_0 \approx 4a$. The discussion in Sec. IV makes clear that neither $F_{\max}$ nor this inferred E are the proper values for Eq. (5), but on the other hand their ratio is what is needed to compute ξ_0 and it is precisely this ratio that is directly measured in the experiments of Sec. IV. We estimate D as the short-time diffusion coefficient, $D \approx k_B T/6\pi\eta a = 0.064\ \mu\mathrm{m}^2/\mathrm{s}$. This approximation using the dilute-limit value is imperfect due to hydrodynamic interactions, which reduce D at larger volume fractions,[59–62] but we are mainly seeking the right order of magnitude. Using this D and ξ_0, we find $\tau \approx 100$ s.

The drag force acting on the magnetic bead is not due to the viscosity η of the solvent (used to calculate D) but rather the effective viscosity of the medium, which is $\approx$50 times larger at these volume fractions.[13] To calculate t_0 we use the more correct value of E estimated from the data of Fig. 1 as discussed in Sec. IV. Using $a_{\mathrm{MB}} = 2.25\ \mu$m and $E = 0.72$ Pa we get $t_0 = 1$ ms. This is too small by a factor of $\sim$200 from the experimental data (Fig. 9). Likewise, given $\tau \approx 100$ s, we would expect to see the asymptotic (stretched exponential) behavior for $\sqrt{(t)} \gg 10$ in Fig. 9: that we see it at earlier time scales suggest that our estimate for τ is too large.

We thus reconsider the correct value of D. In our model, we assume D is the diffusion coefficient for strain. In practice, individual colloidal particles do not need to move significant distances for the strain to diffuse. Much as a dislocation can move rapidly through a crystalline lattice, while individual particles stay close to their lattice sites, a slight motion of a particle ($\Delta r < a$) changes the strain over a neighborhood $\sim a$ in scale. If we assume that particles diffusing a distance of $a/20$ are sufficient for the strain to diffuse a distance a, then D becomes 400 times larger. This decreases τ to 0.2 s and increases t_0 to 0.4 s, bringing our model into more reasonable agreement with the data. The distance $a/20$ is smaller than the cage size (which is about $a/3$).[19]

VI. CONCLUSIONS

We have used magnetic beads to locally perturb a dense colloidal sample at volume fractions $\phi < \phi_g$, close to the colloidal glass transition. The magnetic beads have a linear relationship between the applied forces and their displacement, and the strain field around the beads is well-described as that of a homogeneous elastic medium subject to a point force. The Poisson ratio is $\sigma = 1/2$, consistent with a sample that conserves its total volume when a stress is applied. Not surprisingly, the Young's modulus describing the elastic medium grows as the glass transition is approached. The growth is consistent with power-law in $(\phi_c - \phi)$, where $\phi_c = \phi_{rcp} > \phi_g$.

When the bead is moved away from its equilibrium position and the force is removed, we observed the subsequent relaxation to the equilibrium position. This relaxation behaves as a stretched exponential, $x \sim \exp(-(t/t_0)^{1/2})$. This agrees with a model that assumes the stress can diffuse away to infinity: thus, while the particle is moving back to $x = 0$, the effective spring constant acting on the particle is also diminishing. The experimental time scales suggest that this diffusion is rapid, occurring faster than the particles themselves diffuse. This is likely due to the relatively small displacements of particles needed to change the strain.

ACKNOWLEDGMENTS

We thank R. E. Courtland, S. A. Koehler, M. Fuchs, K. S. Schweizer, and M. Wyart for helpful discussions. We thank A. Schofield for providing our colloidal samples. The work of D.A., D.S., P.H., and J.H. was supported by National Aeronautics and Space Administration (NASA) (Grant No. NAG3-2284). The work of E.R.W. was supported by National Science Foundation (NSF) (Grant No. CHE-0910707).

[1]J. C. Dyre, Rev. Mod. Phys. **78**, 953 (2006).
[2]C. A. Schuh, T. C. Hufnagel, and U. Ramamurty, Acta Mater. **55**, 4067 (2007).
[3]V. Lubchenko and P. G. Wolynes, Annu. Rev. Phys. Chem. **58**, 235 (2007).
[4]A. Cavagna, Phys. Rep. **476**, 51 (2009).
[5]L. Berthier and G. Biroli, Rev. Mod. Phys. **83**, 587 (2011).
[6]F. Léonforte, A. Tanguy, J. P. Wittmer, and J. L. Barrat, Phys. Rev. Lett. **97**, 055501 (2006).
[7]M. Tsamados, A. Tanguy, C. Goldenberg, and J. L. Barrat, Phys. Rev. E **80**, 026112 (2009).
[8]F. Sciortino and P. Tartaglia, Adv. Phys. **54**, 471 (2005).
[9]P. N. Pusey, J. Phys.: Condens. Matter **20**, 494202 (2008).
[10]G. L. Hunter and E. R. Weeks, Rep. Prog. Phys. **75**, 066501 (2012).
[11]P. N. Pusey and W. van Megen, Nature (London) **320**, 340 (1986).
[12]C. P. Royall, W. C. K. Poon, and E. R. Weeks, Soft Matter **9**, 17 (2013).
[13]Z. Cheng, J. Zhu, P. M. Chaikin, S.-E. Phan, and W. B. Russel, Phys. Rev. E **65**, 041405 (2002).
[14]S. Torquato, T. M. Truskett, and P. G. Debenedetti, Phys. Rev. Lett. **84**, 2064 (2000).
[15]J. D. Bernal, Proc. R. Soc. London, Ser. A **280**, 299 (1964).
[16]T. G. Mason and D. A. Weitz, Phys. Rev. Lett. **75**, 2770 (1995).
[17]E. Rabani, J. D. Gezelter, and B. J. Berne, J. Chem. Phys. **107**, 6867 (1997).
[18]B. Doliwa and A. Heuer, Phys. Rev. Lett. **80**, 4915 (1998).
[19]E. R. Weeks and D. A. Weitz, Chem. Phys. **284**, 361 (2002).
[20]K. S. Schweizer and E. J. Saltzman, J. Chem. Phys. **119**, 1181 (2003).
[21]K. S. Schweizer and G. Yatsenko, J. Chem. Phys. **127**, 164505 (2007).
[22]D. M. Sussman and K. S. Schweizer, J. Chem. Phys. **134**, 064516 (2011).
[23]C. J. Harrer, A. M. Puertas, T. Voigtmann, and M. Fuchs, Z. Phys. Chem. **226**, 779 (2012).
[24]S. R. Williams and D. J. Evans, Phys. Rev. Lett. **96**, 015701 (2006).
[25]I. Gazuz, A. M. Puertas, T. Voigtmann, and M. Fuchs, Phys. Rev. Lett. **102**, 248302 (2009).
[26]M. V. Gnann, I. Gazuz, A. M. Puertas, M. Fuchs, and T. Voigtmann, Soft Matter **7**, 1390 (2011).
[27]D. Winter, J. Horbach, P. Virnau, and K. Binder, Phys. Rev. Lett. **108**, 028303 (2012).
[28]M. V. Gnann and T. Voigtmann, Phys. Rev. E **86**, 011406 (2012).
[29]M. B. Hastings, C. J. O. Reichhardt, and C. Reichhardt, Phys. Rev. Lett. **90**, 098302 (2003).
[30]P. Habdas, D. Schaar, A. C. Levitt, and E. R. Weeks, Europhys. Lett. **67**, 477 (2004).
[31]I. C. Carpen and J. F. Brady, J. Rheol. **49**, 1483 (2005).
[32]C. Reichhardt and C. J. O. Reichhardt, Phys. Rev. Lett. **96**, 028301 (2006).
[33]C. J. O. Reichhardt and C. Reichhardt, Phys. Rev. E **82**, 051306 (2010).
[34]J. A. Drocco, M. B. Hastings, C. J. O. Reichhardt, and C. Reichhardt, Phys. Rev. Lett. **95**, 088001 (2005).
[35]L. Antl, J. W. Goodwin, R. D. Hill, R. H. Ottewill, S. M. Owens, S. Papworth, and J. A. Waters, Colloids Surf. **17**, 67 (1986).
[36]A. D. Dinsmore, E. R. Weeks, V. Prasad, A. C. Levitt, and D. A. Weitz, Appl. Opt. **40**, 4152 (2001).
[37]J. C. Crocker and D. G. Grier, J. Colloid Interface Sci. **179**, 298 (1996).
[38]W. C. K. Poon, E. R. Weeks, and C. P. Royall, Soft Matter **8**, 21 (2012).
[39]T. M. Squires and J. F. Brady, Phys. Fluids **17**, 073101 (2005).
[40]A. S. Khair and J. F. Brady, J. Fluid Mech. **557**, 73 (2006).
[41]A. Meyer, A. Marshall, B. G. Bush, and E. M. Furst, J. Rheol. **50**, 77 (2006).
[42]L. G. Wilson, A. W. Harrison, A. B. Schofield, J. Arlt, and W. C. K. Poon, J. Phys. Chem. B **113**, 3806 (2009).
[43]I. Sriram, A. Meyer, and E. M. Furst, Phys. Fluids **22**, 062003 (2010).
[44]L. G. Wilson, A. W. Harrison, W. C. K. Poon, and A. M. Puertas, Europhys. Lett. **93**, 58007 (2011).
[45]E. R. Weeks, in *Experimental and Computational Techniques in Soft Condensed Matter Physics*, edited by J. S. Olafsen (Cambridge University Press, 2010), pp. 1–24.
[46]L. D. Landau, L. P. Pitaevskii, E. M. Lifshitz, and A. M. Kosevich, *Theory of Elasticity*, 3rd ed. (Butterworth-Heinemann, 1986).
[47]D. J. Durian, Phys. Rev. Lett. **75**, 4780 (1995).
[48]D. J. Durian, Phys. Rev. E **55**, 1739 (1997).
[49]C. S. O'Hern, L. E. Silbert, A. J. Liu, and S. R. Nagel, Phys. Rev. E **68**, 011306 (2003).
[50]C. Brito and M. Wyart, Europhys. Lett. **76**, 149 (2006).
[51]A. Tanguy, J. P. Wittmer, F. Leonforte, and J. L. Barrat, Phys. Rev. B **66**, 174205 (2002).
[52]J. P. Wittmer, A. Tanguy, J. L. Barrat, and L. Lewis, Europhys. Lett. **57**, 423 (2002).
[53]F. Leonforte, R. Boissière, A. Tanguy, J. P. Wittmer, and J. L. Barrat, Phys. Rev. B **72**, 224206 (2005).
[54]W. G. Ellenbroek, E. Somfai, M. van Hecke, and W. van Saarloos, Phys. Rev. Lett. **97**, 258001 (2006).
[55]C. Brito and M. Wyart, J. Stat. Mech.: Theory Exp. **2007**, L08003.
[56]A. Widmer-Cooper, H. Perry, P. Harrowell, and D. R. Reichman, Nat. Phys. **4**, 711 (2008).
[57]R. Candelier, A. Widmer-Cooper, J. K. Kummerfeld, O. Dauchot, G. Biroli, P. Harrowell, and D. R. Reichman, Phys. Rev. Lett. **105**, 135702 (2010).
[58]M. L. Manning and A. J. Liu, Phys. Rev. Lett. **107**, 108302 (2011).
[59]P. N. Pusey and R. J. A. Tough, Faraday Discuss. Chem. Soc. **76**, 123 (1983).
[60]I. Snook, W. van Megen, and R. J. A. Tough, J. Chem. Phys. **78**, 5825 (1983).
[61]C. W. J. Beenakker and P. Mazur, Phys. Lett. A **98**, 22 (1983).
[62]C. W. J. Beenakker and P. Mazur, Physica A **126**, 349 (1984).